


# Thermodynamic properties of argon from Monte Carlo simulations using *ab initio* potentials

Philipp Ströker<sup>1</sup>,\* Robert Hellmann<sup>1,†</sup> and Karsten Meier<sup>1,‡</sup>

*Institut für Thermodynamik, Helmut-Schmidt-Universität/Universität der Bundeswehr Hamburg,  
Holstenhofweg 85, 22043 Hamburg, Germany*

 (Received 11 January 2022; accepted 16 May 2022; published 28 June 2022)

Ten different thermodynamic properties of the noble gas argon in the liquid and supercritical regions were obtained from semiclassical Monte Carlo simulations in the isothermal-isobaric ensemble using *ab initio* potentials for the two-body and nonadditive three-body interactions. Our results for the density and speed of sound agree with the most accurate experimental data for argon almost within the uncertainty of these data, a level of agreement unprecedented for many-particle simulations. This demonstrates the high predictive but yet unexploited power of *ab initio* potentials in the field of molecular modeling and simulation for thermodynamic properties of fluids.

DOI: [10.1103/PhysRevE.105.064129](https://doi.org/10.1103/PhysRevE.105.064129)

## I. INTRODUCTION

Noble gases are the most important model substances for theory of thermophysical properties of fluids. Because of their monatomic structure and spherical symmetry, it is possible to apply essentially exact statistical-mechanical theories in combination with accurate models for interatomic interactions for the calculation of their properties. Among the noble gases, argon is the most well studied concerning thermodynamic properties.

Molecular simulations for argon with accurate empirical or *ab initio* potentials were conducted by Huber and coworkers [1–3], Anta *et al.* [4], Deiters and coworkers [5,6], Nasrabad and Laghaei [7], Bukowski and Szalewicz [8], Sadus and coworkers [9–14], Malijevský and Malijevský [15], Pahl *et al.* [16], and Deiters and Sadus [17,18]. Mostly, the vapor-liquid equilibrium was examined by the Gibbs ensemble method [4–10,13,18]. Sometimes, single-phase thermodynamic properties [7,8,12,14,15,17], transport coefficients [1], structural properties [1,3,8], or the solid-liquid equilibrium [2,11,16,18] were investigated. These studies revealed that nonadditive three-body interactions yield significant contributions to the vapor-liquid equilibrium and single-phase properties. However, the results remained qualitative and deviate from accurate experimental data by several percent or more. The simulations often suffered from finite-size effects due to small particle numbers, poor statistics due to short simulation runs, and crude models for nonadditive three-body interactions, such as the Axilrod-Teller-Muto (ATM) potential [19,20] if an explicit three-body model was considered at all.

Traditionally, molecular simulations have also been hampered by the unavailability of a systematic and complete statistical-mechanical theory for calculating all thermody-

amic properties. Lustig devised such a theory for the microcanonical and canonical ensembles [21–27]. We recently extended Lustig’s work to the isothermal-isobaric ensemble [28]. Its main advantage over isochoric ensembles is that the expressions for thermodynamic properties contain only combinations of the enthalpy and volume but no volume derivatives of the enthalpy. To evaluate volume derivatives, derivatives of the potential with respect to the interparticle separations are required. Thus, avoiding volume derivatives reduces the implementation effort and improves the computational efficiency. As the first major application of our extension of Lustig’s work, we demonstrate the transformative performance of this approach in combination with state-of-the-art *ab initio* potentials and semiclassically considered nuclear quantum effects by Monte Carlo simulations of liquid and supercritical argon that are extremely precise and essentially free of finite-size effects.

This article is organized as follows. Section II describes the potential models used in the simulations. Section III provides the equations for the calculation of the thermodynamic properties in the isothermal-isobaric ensemble, and Sec. IV summarizes details of our Monte Carlo simulations. The results of our simulations are reported and discussed in Sec. V. Conclusions and recommendations for future work are presented in Sec. VI.

## II. POTENTIAL MODELS

In our simulations, the total interaction potential  $V$  of the system is based on the exact many-body expansion

$$V = \sum_{i<j}^N v_{ij} + \sum_{i<j<k}^N \Delta v_{ijk} + \sum_{i<j<k<l}^N \Delta v_{ijkl} + \dots, \quad (1)$$

where  $N$  is the number of particles,  $v_{ij}$  denotes the pair potential between particles  $i$  and  $j$ ,  $\Delta v_{ijk}$  is the nonadditive three-body potential between particles  $i$ ,  $j$ , and  $k$ , and so forth.

\*philipp.stroeker@hsu-hh.de

†robert.hellmann@hsu-hh.de

‡karsten.meier@hsu-hh.de

The nonadditive three-body potential  $\Delta v_{ijk}$  is defined as

$$\Delta v_{ijk} = v_{ijk} - v_{ij} - v_{ik} - v_{jk}, \quad (2)$$

where  $v_{ijk}$  denotes the total interaction potential of three particles. Since Eq. (1) converges rapidly in simple atomic or molecular fluids and because the computational effort increases dramatically with each new term in the expansion, we only considered two-body and nonadditive three-body interactions.

For the pair interactions, we used the highly accurate *ab initio* potential of Jäger *et al.* [29],

$$v_{2B}(r) = A \exp(a_1 r + a_2 r^2 + a_{-1} r^{-1} + a_{-2} r^{-2}) - \sum_{n=3}^8 \frac{C_{2n}}{r^{2n}} \left( 1 - \exp(-br) \sum_{k=0}^{2n} \frac{(br)^k}{k!} \right), \quad (3)$$

where  $r$  is the separation between two argon atoms, and  $A$ ,  $a_1$ ,  $a_2$ ,  $a_{-1}$ ,  $a_{-2}$ ,  $b$ , and  $C_{2n}$  are parameters given in the original publication. Jäger *et al.* fitted the analytical potential function to interaction energies obtained from high-level quantum-chemical *ab initio* calculations. Since the analytical pair potential function exhibits a spurious maximum at a very small, thermally unreachable separation, hard spheres with a radius of 1.8 Å were placed on the atoms to avoid sampling of this unphysical region of the potential.

We accounted for nuclear quantum effects semiclassically by adding Feynman-Hibbs (FH) corrections [30] to the pair potential. For spherical particles, such as argon atoms, the second-order correction is given by

$$v_{\text{FH}}(r, T) = \frac{\hbar^2}{12mk_B T} \left[ \frac{\partial^2 v_{2B}(r)}{\partial r^2} + \frac{2}{r} \frac{\partial v_{2B}(r)}{\partial r} \right], \quad (4)$$

where  $m$  is the mass of a particle,  $k_B$  is the Boltzmann constant,  $\hbar$  is Planck's constant divided by  $2\pi$ , and  $T$  denotes temperature. Since the correction is inversely proportional to  $T$ , its influence increases with decreasing temperature. Test simulations verified that the fourth-order correction can be safely neglected. Vogel *et al.* [31] showed that second density, acoustic, and dielectric virial coefficients and the viscosity and thermal conductivity in the zero-density limit calculated with the pair potential of Jäger *et al.* and corrections for quantum effects agree excellently with the most accurate experimental data.

To account for nonadditive three-body interactions, we again used an *ab initio* potential of Jäger *et al.* [32]. Their potential is represented as a sum of an exponential contribution,  $\Delta v_{3B}^{\text{exp}}$ , and of a damped third-order dispersion contribution,  $\Delta v_{3B}^{\text{disp}}$ . The exponential part is given by

$$\begin{aligned} \Delta v_{3B}^{\text{exp}}(r_{12}, r_{23}, r_{31}) &= \sum_{\substack{k_1+k_2+k_3 \leq 6 \\ 0 \leq k_1 \leq k_2 \leq k_3}} A_{k_1 k_2 k_3} \exp[-\alpha_{k_1 k_2 k_3} (r_{12} + r_{23} + r_{31})] \\ &\times \mathfrak{P}[P_{k_1}(\cos \theta_1) P_{k_2}(\cos \theta_2) P_{k_3}(\cos \theta_3)], \end{aligned} \quad (5)$$

where  $r_{ij}$  is the separation between atoms  $i$  and  $j$ ,  $\theta_i$  is the interior angle at atom  $i$  in the triangle formed by the three atoms, the operator  $\mathfrak{P}$  sums over all six permutations of the interior angles, and  $P_k$  denotes the Legendre polynomial of

order  $k$ . The dispersion contribution is represented by

$$\begin{aligned} \Delta v_{3B}^{\text{disp}}(r_{12}, r_{23}, r_{31}) &= \sum'_{\substack{l_1, l_2, l_3=1 \\ l_1+l_2+l_3 \leq 6}}^3 D(\beta_{l_1 l_2 l_3}, r_{12}, r_{23}, r_{31}) W_{l_1 l_2 l_3}^{(3)} Z_{l_1 l_2 l_3}^{(3)}, \end{aligned} \quad (6)$$

where the prime indicates that the summation omits the term  $(l_1 l_2 l_3) = (123)$  and its permutations. The damping functions  $D$  are defined as

$$\begin{aligned} D(\beta_{l_1 l_2 l_3}, r_{12}, r_{23}, r_{31}) &= D(\beta_{l_1 l_2 l_3}, r_{12}) D(\beta_{l_1 l_2 l_3}, r_{23}) D(\beta_{l_1 l_2 l_3}, r_{31}), \end{aligned} \quad (7)$$

where the factors on the right-hand side are Tang-Toennies damping functions [33]:

$$D(\beta_{l_1 l_2 l_3}, r_{ij}) = 1 - \exp(-\beta_{l_1 l_2 l_3} r_{ij}) \sum_{n=0}^{n_{ij}^{l_1 l_2 l_3}} \frac{(\beta_{l_1 l_2 l_3} r_{ij})^n}{n!}. \quad (8)$$

Here  $n_{ij}^{l_1 l_2 l_3}$  is the inverse power to which  $r_{ij}$  is raised in the function  $W_{l_1 l_2 l_3}^{(3)}$ . The first summand on the right-hand side of Eq. (6) with  $l_1 = l_2 = l_3 = 1$  is the triple-dipole term given by

$$W_{111}^{(3)} = 3(r_{12} r_{23} r_{31})^{-3} (1 + 3 \cos \theta_1 \cos \theta_2 \cos \theta_3). \quad (9)$$

Except for a numerical prefactor,  $W_{111}^{(3)}$  corresponds to the simple ATM model [19,20]. The other functions  $W_{l_1 l_2 l_3}^{(3)}$  and the numerical values of the parameters of the potential,  $A_{k_1 k_2 k_3}$ ,  $\alpha_{k_1 k_2 k_3}$ ,  $\beta_{l_1 l_2 l_3}$ , and  $Z_{l_1 l_2 l_3}^{(3)}$  (56 parameters in total), are given in Ref. [32]. Jäger *et al.* [32] showed that the third virial coefficient of argon can be determined quantitatively only if the *ab initio* nonadditive three-body potential is included. Considering the pair potential and its FH correction alone is insufficient.

Jäger *et al.* [32,34] also developed a seventh-order virial equation of state (VEOS) based on the above-mentioned potential models. This VEOS agrees very well with experimental data for the density and speed of sound of argon in the gas region and a part of the supercritical region where the VEOS is sufficiently converged, thus providing additional confirmation of the high quality of the pair and nonadditive three-body potentials developed by Jäger *et al.* [29,32]. At a few state points, we also tested the more recent *ab initio* nonadditive three-body potential of Cenek *et al.* [35].

We performed the Monte Carlo simulations at three different levels of sophistication. In the first model, 2B, solely the *ab initio* pair potential of Jäger *et al.* [29] was used. In the second model, 2B+3B, the *ab initio* nonadditive three-body potential of Jäger *et al.* [32] was added to the pair potential. In the third model, 2B+FH+3B, additional quantum effects were taken into account semiclassically through the second-order FH correction to the pair potential. In a fourth model, 2B+FH+3B/C, the *ab initio* potential of Cenek *et al.* [35] was used to account for nonadditive three-body interactions.

### III. EQUATIONS FOR THERMODYNAMIC PROPERTIES

Our Monte Carlo simulations were carried out in the isothermal-isobaric ensemble, in which the number of particles  $N$ , the pressure  $p$ , and the temperature  $T$  are the

independent variables. In the following, we provide a brief summary of the equations employed for the calculation of thermodynamic properties in this work. A detailed derivation of these equations can be found in our previous work [28].

In the  $NpT$  ensemble, the Gibbs energy  $G$  is the thermodynamic potential. It is related to the partition function of the  $NpT$  ensemble

$$Z(N, p, T) = \frac{N}{N! h^{3N}} \int_0^\infty \iint e^{-\beta(E+pV)} V^{-1} d\mathbf{p}^N d\mathbf{r}^N dV \quad (10)$$

by

$$G = -k_B T \ln Z(N, p, T) = -\beta^{-1} \ln Z(N, p, \beta). \quad (11)$$

In these equations,  $h$  is the Planck constant,  $E$  is the internal energy of the system,  $V$  is the volume,  $d\mathbf{p}^N$  and  $d\mathbf{r}^N$  represent  $3N$ -fold integrations over the momenta and coordinates of the particles, and  $\beta = 1/k_B T$  is introduced as an abbreviation. For a systematic representation of thermodynamic properties, phase-space functions

$$Z_{mn} = \frac{1}{Z} \frac{\partial^{m+n} Z}{\partial \beta^m \partial p^n}, \quad m, n = 0, 1, 2, \dots, \quad (12)$$

are introduced, which are related to derivatives of the partition function  $Z$  with respect to temperature and pressure. In this work, the density  $\rho$ , enthalpy  $H$ , isobaric heat capacity  $C_p$ , isochoric heat capacity  $C_V$ , isobaric expansion coefficient  $\alpha_p$ , isochoric pressure coefficient  $\gamma_V$ , isothermal compressibility  $\beta_T$ , isentropic compressibility  $\beta_S$ , speed of sound  $w$ , and Joule-Thomson coefficient  $\mu_{JT}$  were calculated. The expressions for the density, enthalpy, isobaric heat capacity, isochoric heat capacity, isobaric expansion coefficient, and isothermal compressibility in terms of phase-space functions read

$$\rho = -\frac{\beta N}{Z_{01}}, \quad (13)$$

$$H = -Z_{10}, \quad (14)$$

$$C_p = k_B \beta^2 (Z_{20} - Z_{10}^2), \quad (15)$$

$$C_V = k_B \left\{ \beta^2 (Z_{20} - Z_{10}^2) - \frac{[Z_{01} - \beta(Z_{11} - Z_{10}Z_{01})]^2}{Z_{02} - Z_{01}^2} \right\}, \quad (16)$$

$$\alpha_p = \frac{k_B \beta}{Z_{01}} [Z_{01} - \beta(Z_{11} - Z_{10}Z_{01})], \quad (17)$$

$$\beta_T = -\frac{Z_{02} - Z_{01}^2}{Z_{01}}. \quad (18)$$

When these properties are known, the thermal pressure coefficient  $\gamma_V = \alpha_p/\beta_T$ , the isentropic compressibility  $\beta_S = \beta_T C_V/C_p$ , the speed of sound  $w = (V/NM\beta_S)^{1/2}$  with the molar mass of krypton  $M = 83.798 \text{ kg kmol}^{-1}$ , and the Joule-Thomson coefficient  $\mu_{JT} = V(T\alpha_p - 1)/C_p$  can be calculated. The phase-space functions required in Eqs. (13) to (18) are given in Table I. In simulations with models 2B+FH+3B and 2B+FH+3B/C, the phase-space functions  $Z_{mn}^{\text{TDP}}$  for temperature-dependent potentials were applied.

#### IV. SIMULATION PROTOCOL

The simulations were performed in the isothermal-isobaric ensemble using the Metropolis algorithm [36] as described in our previous work [28]. Depending on the number of particles, they were either initiated from a face-centered, body-centered, or simple cubic lattice and carried out in a cubic box under periodic boundary conditions and the minimum image convention. The Markov chain was divided into cycles consisting of  $N$  trials each. On average, one volume change and  $N - 1$  particle displacements were attempted per cycle. The type of move was selected randomly to fulfill detailed balance. The maximum particle displacement and volume change were adjusted during the simulation such that the acceptance ratio for both types of moves was approximately 50%. In all simulations, the cutoff radius was set to half the box length. After an equilibration phase of  $10^5$  cycles, the production phase of each simulation extended over  $10^7$  cycles.

The three-body contribution was set to zero if the separation between one pair of particles in a triplet was smaller than  $2.25 \text{ \AA}$  because its relative contribution in this range becomes negligible. To reduce the computational cost for the evaluation of the nonadditive three-body potentials, three-dimensional interpolation tables with the separations between two pairs of argon atoms and the enclosed angle as independent variables were applied. The grid consisted of 600 points in each dimension and extended from  $2.25 \text{ \AA}$  to the cutoff radius of the potentials. Interpolation was performed using a multivariate cubic Lagrange interpolation scheme. Relative differences between values calculated with the analytical potentials and

TABLE I. Explicit expressions for phase-space functions  $Z_{mn}$  and  $Z_{mn}^{\text{TDP}}$  up to second order for ordinary and temperature-dependent potentials, respectively, in the  $NpT$  ensemble. Angular brackets denote ensemble averages, and  $U$  is the potential energy.

---



---

$Z_{10} = -\frac{3N}{2} \beta^{-1} - \langle U + pV \rangle$
$Z_{20} = \frac{3N}{2} \left( \frac{3N}{2} + 1 \right) \beta^{-2} + 3N \beta^{-1} \langle U + pV \rangle + \langle (U + pV)^2 \rangle$
$Z_{01} = -\beta \langle V \rangle$
$Z_{02} = \beta^2 \langle V^2 \rangle$
$Z_{11} = \left( \frac{3N}{2} - 1 \right) \langle V \rangle + \beta \langle (U + pV)V \rangle$
$Z_{10}^{\text{TDP}} = -\frac{3N}{2} \beta^{-1} - \langle U(\beta) + \beta \frac{\partial U(\beta)}{\partial \beta} + pV \rangle$
$Z_{20}^{\text{TDP}} = \frac{3N}{2} \left( \frac{3N}{2} + 1 \right) \beta^{-2} + 3N \beta^{-1} \langle U(\beta) + \beta \frac{\partial U(\beta)}{\partial \beta} + pV \rangle + \langle (U(\beta) + \beta \frac{\partial U(\beta)}{\partial \beta} + pV)^2 \rangle - \langle 2 \frac{\partial U(\beta)}{\partial \beta} + \beta \frac{\partial^2 U(\beta)}{\partial \beta^2} \rangle$
$Z_{11}^{\text{TDP}} = \left( \frac{3N}{2} - 1 \right) \langle V \rangle + \beta \langle (U(\beta) + \beta \frac{\partial U(\beta)}{\partial \beta} + pV)V \rangle$

---



---

the interpolation tables were typically less than 0.5 parts per million. Even with these performance improvements, one simulation run with 500 particles and model 2B+FH+3B still required about 40 days on a 28-core compute node.

The contributions of interactions between particles beyond the cutoff radius to the total pair interaction potential were calculated as described by Allen and Tildesley [37] using an interpolation table to avoid having to recompute the cutoff correction after each volume change. Depending on the model, the correction was applied to the pair potential either with or without the FH correction. Since the contribution of nonadditive three-body interactions is much smaller than that of two-body interactions and because the three-body potential decays rapidly with increasing separations between the atoms, the long-range correction to the nonadditive three-body potential was neglected. Moreover, the latter correction vanishes when we extrapolate the results for thermodynamic properties obtained by simulations with different particle numbers into the thermodynamic limit.

## V. RESULTS AND DISCUSSION

Simulations were carried out along the liquid isotherm 100 K between 1 and 68 MPa and at the supercritical isotherm 300 K from 10 to 100 MPa at six state points for each isotherm. Since the system remained in a solid state at 100 K when the simulation was initiated from a lattice configuration, the system was melted with a short simulation at 400 K before proceeding with the equilibration phase. As it was the aim to simulate properties of macroscopic systems, simulations with 64, 80, 108, 128, 160, 216, 256, and 500 particles for the models 2B and 2B+FH+3B were performed at each state point, and the results were extrapolated into the thermodynamic limit, i.e., to an infinite number of particles. The extrapolated values for the properties were obtained by a weighted linear least-squares fit to the results of the simulations as a function of the inverse number of particles. With models 2B+3B and 2B+FH+3B/C, simulations were only performed at the lowest and highest pressures on both isotherms. In each simulation, we calculated the density  $\rho$ , specific enthalpy  $h$ , specific isochoric heat capacity  $c_V$ , specific isobaric heat capacity  $c_p$ , thermal pressure coefficient  $\gamma_V$ , thermal expansion coefficient  $\alpha_p$ , isothermal compressibility  $\beta_T$ , isentropic compressibility  $\beta_S$ , Joule-Thomson coefficient  $\mu_{JT}$ , and speed of sound  $w$  by applying the equations given in Sec. III. We note that for argon most of these properties have never been simulated before with explicit consideration of three-body interactions.

The uncertainty in the results of a simulation was determined by the block average method. Subsequently, the extrapolated values and their uncertainties were determined by the Monte Carlo method proposed in Supplement 1 to the ‘‘Guide to the Expression of Uncertainty in Measurement’’ (GUM) [38]. In this work, all uncertainties are reported as expanded uncertainties (coverage factor  $k = 2$ ). To illustrate the extrapolation of the simulation results into the thermodynamic limit, Fig. 1 exemplarily shows results for the density at (300 K, 10 MPa) and (100 K, 68 MPa) for models 2B, 2B+3B, and 2B+FH+3B as a function of the inverse particle

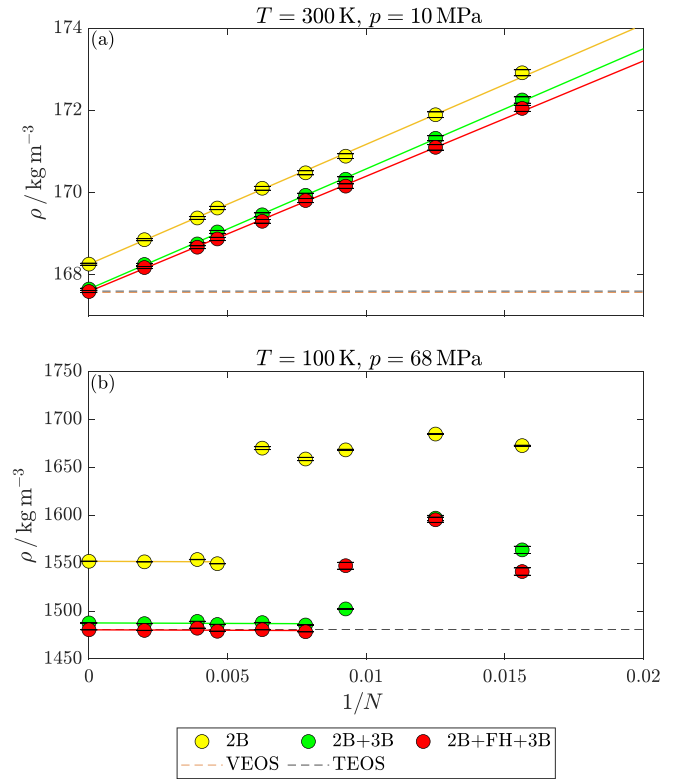


FIG. 1. Results of the Monte Carlo simulations and extrapolated values in the thermodynamic limit for the density at (a) (300 K, 10 MPa) and (b) (100 K, 68 MPa) for models 2B, 2B+3B, and 2B+FH+3B vs the inverse particle number. Solid lines represent linear fits to the data.

number. Figures showing the extrapolation of all properties at both simulated isotherms are provided in the Supplemental Material [39]. At (300 K, 10 MPa), the density decreases linearly into the thermodynamic limit; i.e., linear fits provide a good representation of the data. The extrapolated value for model 2B+FH+3B agrees with the reference equation of state by Tegeler *et al.* [40] for argon (TEOS) within 0.0063% and with the VEOS within 0.0031%, which is well within the simulation uncertainty. Since the VEOS is also based on model 2B+FH+3B, this level of agreement verifies that our Monte Carlo algorithm was implemented correctly.

At (100 K, 68 MPa) near the freezing line, the situation is more complicated. Densities obtained from the simulations with small particle numbers, e.g., with 64, 80, and 108 particles for model 2B+FH+3B, are up to 7.9% higher than those obtained with large particle numbers. The higher results for small particle numbers show that the system was at least partially solid. Therefore, the extrapolation was performed only with the results for larger particle numbers.

The extrapolated simulation results for all properties for model 2B+FH+3B at all simulated state points are reported in Tables II and III. The results for models 2B, 2B+3B and 2B+FH+3B/C are provided in the Supplemental Material [39]. Figure 2 depicts relative deviations of the results for the density, isochoric heat capacity, and speed of sound for models 2B, 2B+3B, and 2B+FH+3B from the TEOS. Similar deviation plots for the other properties are also provided in the Supplemental Material. At 100 K, the nonadditive

TABLE II. Results for thermodynamic properties of argon at the isotherm 100 K obtained with model 2B+FH+3B. Numbers in parentheses represent expanded statistical uncertainties (coverage factor  $k = 2$ ) in the rightmost digits of the value.

$p/\text{MPa}$	1	10	20	30	50	68
$\rho/\text{kg m}^{-3}$	1316.52(20)	1349.35(19)	1379.40(17)	1405.29(16)	1448.22(15)	1480.45(14)
$h/\text{kJ kg}^{-1}$	-103.576(23)	-100.073(23)	-95.784(22)	-91.285(22)	-81.808(23)	-72.992(25)
$c_V/\text{kJ (kg K)}^{-1}$	0.4993(5)	0.5101(5)	0.5205(6)	0.5301(7)	0.5465(8)	0.5597(10)
$c_p/\text{kJ (kg K)}^{-1}$	1.149(7)	1.101(7)	1.065(6)	1.037(6)	0.997(6)	0.975(6)
$\gamma_V/\text{MPa K}^{-1}$	1.6682(32)	1.8054(38)	1.9290(45)	2.035(5)	2.207(7)	2.340(8)
$\alpha_p/\text{K}^{-1}$	0.005130(48)	0.004419(39)	0.003895(34)	0.003504(30)	0.002957(26)	0.002624(25)
$\beta_T/\text{MPa}^{-1}$	0.003075(25)	0.002447(18)	0.002020(14)	0.001722(11)	0.001339(8)	0.001121(7)
$\beta_S/\text{MPa}^{-1}$	0.0013366(38)	0.0011336(28)	0.0009870(23)	0.0008797(20)	0.0007342(16)	0.0006435(14)
$w/\text{m s}^{-1}$	753.7(10)	808.3(10)	856.8(10)	899.1(10)	969.5(10)	1024.2(11)
$\mu_{JT}/\text{K MPa}^{-1}$	-0.322(5)	-0.375(5)	-0.4152(49)	-0.4453(47)	-0.4876(48)	-0.5118(48)

three-body interactions yield the largest contribution to the three properties near the vapor-liquid phase boundary. They reduce  $\rho$  by up to 7.1%,  $c_V$  by up to 6.4%, and  $w$  by up to 13%. The FH correction contributes up to  $-0.72\%$ ,  $-2.2\%$ , and  $-1.2\%$ , respectively. At 300 K, the contribution of the nonadditive three-body interactions increases with pressure, but it is smaller than at 100 K. It amounts to up to  $-3.3\%$  for  $\rho$ , up to  $-1.2\%$  for  $c_V$ , and up to  $-0.77\%$  for  $w$ . The FH correction contributes up to 0.15% to  $\rho$ , up to 0.21% to  $c_V$ , and up to 0.12% to  $w$ . These results demonstrate that nonadditive three-body interactions and corrections for quantum effects are essential for extracting thermodynamic properties with low uncertainties from simulations with *ab initio* potentials. In order to compare our results for model 2B+FH+3B with the most accurate experimental data and the TEOS, Fig. 3 depicts relative deviations from the TEOS with higher resolution. Also shown are relative deviations of the experimental data of Gilgen *et al.* (uncertainty: 0.015–0.02%) [41], Klimeck *et al.* (uncertainty: 0.02%) [42], and Michels *et al.* (uncertainty: 0.10–0.15%) [43] for  $\rho$  and of Estrada-Alexanders and Trusler (uncertainty: 0.001–0.007%) [44], Streett and Constantino (uncertainty: 0.2%) [45], Thoen *et al.* (uncertainty: 0.07%) [46], and Meier and Kabelac (uncertainty: 0.014%) [47] for  $w$ .

Our results for  $\rho$  have uncertainties between 0.009% and 0.016%. At 100 K below 12 MPa, they agree with the TEOS within 0.005% and within 0.023% at higher pressures. At 300 K, the two data points at 10 and 20 MPa agree with the

TEOS within 0.009%, but at higher pressures the deviations increase and reach 0.06% at 100 MPa. The data at low pressures also agree with the experimental data of Gilgen *et al.* and Klimeck *et al.* within their uncertainty. The experimental data of Michels *et al.* at 300 K are up to 0.1% higher than our values.

Since there are no low-uncertainty experimental data for the isochoric heat capacity, we compare our results only with the TEOS. The results for  $c_V$  at 100 K have uncertainties of 0.10–0.17% and agree with the TEOS within 0.62%. At 300 K, the uncertainty is less than 0.02%, and the data agree with the TEOS within 0.06%. This agreement is well within the rather high uncertainty of the TEOS.

Our results for the speed of sound have an uncertainty of at most 0.14% and agree with the TEOS within 0.3% at 100 K and within 0.08% at 300 K. At 300 K, our results almost coincide with the data of Estrada-Alexanders and Trusler and the data of Meier and Kabelac at 10, 20, 40, and 80 MPa. The values at 60 and 100 MPa deviate by  $-0.06\%$  from the data of Meier and Kabelac, but the agreement is within our uncertainties. At 100 K, our results agree well with the data of Thoen *et al.*, but are up to 0.3% higher than those of Streett and Constantino.

Our results for  $\rho$  obtained with model 2B+FH+3B/C deviate by up to  $-0.13\%$  from those for model 2B+FH+3B, whereas for  $c_V$  and  $w$  the two models are consistent within their uncertainties.

TABLE III. Results for thermodynamic properties of argon at the isotherm 300 K obtained with model 2B+FH+3B. Numbers in parentheses represent expanded statistical uncertainties (coverage factor  $k = 2$ ) in the rightmost digits of the value.

$p/\text{MPa}$	10	20	40	60	80	100
$\rho/\text{kg m}^{-3}$	167.592(25)	335.81(5)	599.97(10)	766.90(10)	880.28(10)	964.26(9)
$h/\text{kJ kg}^{-1}$	137.977(11)	123.166(14)	108.067(19)	105.915(18)	109.447(18)	115.745(17)
$c_V/\text{kJ (kg K)}^{-1}$	0.329051(46)	0.341642(33)	0.35716(5)	0.36869(6)	0.37920(7)	0.38880(8)
$c_p/\text{kJ (kg K)}^{-1}$	0.6478(7)	0.7581(12)	0.8251(15)	0.8111(14)	0.7896(14)	0.7760(13)
$\gamma_V/\text{MPa K}^{-1}$	0.041665(15)	0.098808(31)	0.23244(9)	0.35876(15)	0.46995(21)	0.56842(28)
$\alpha_p/\text{K}^{-1}$	0.004272(9)	0.004717(13)	0.004026(13)	0.003152(10)	0.002562(8)	0.002189(7)
$\beta_T/\text{MPa}^{-1}$	0.10254(23)	0.04774(12)	0.01732(5)	0.008785(26)	0.005452(16)	0.003851(11)
$\beta_S/\text{MPa}^{-1}$	0.05208(6)	0.021516(25)	0.007497(10)	0.003993(5)	0.0026182(34)	0.0019297(25)
$w/\text{m s}^{-1}$	338.42(20)	372.02(22)	471.53(32)	571.46(37)	658.73(43)	733.13(47)
$\mu_{JT}/\text{K MPa}^{-1}$	2.596(23)	1.631(12)	0.420(7)	-0.0875(49)	-0.3328(40)	-0.4588(35)

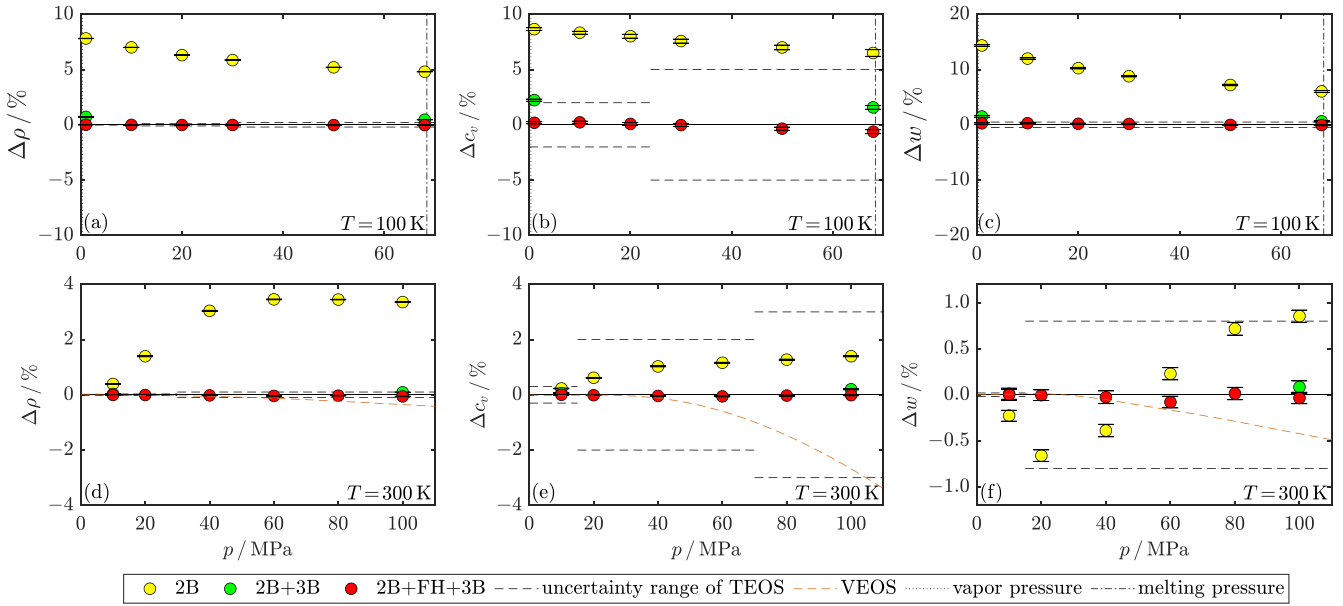


FIG. 2. Relative deviations of our results for the density, isochoric heat capacity, and speed of sound for models 2B, 2B+3B, and 2B+FH+3B at 100 and 300 K from the TEOS as a function of pressure  $p$  (a)–(f).

VI. CONCLUSIONS

In summary, our results for model 2B+FH+3B agree with the TEOS and the most accurate experimental data for the density and speed of sound within our low uncertainty, thus demonstrating that it is possible to determine thermodynamic properties of noble gases by Monte Carlo simulations using

state-of-the-art *ab initio* potentials with an uncertainty comparable to that achieved by the most accurate experimental techniques.

There are several points worth recommending for the accurate determination of thermodynamic properties of fluids by Monte Carlo simulations in future work. First, the rigorous expressions for thermodynamic properties in the simulated

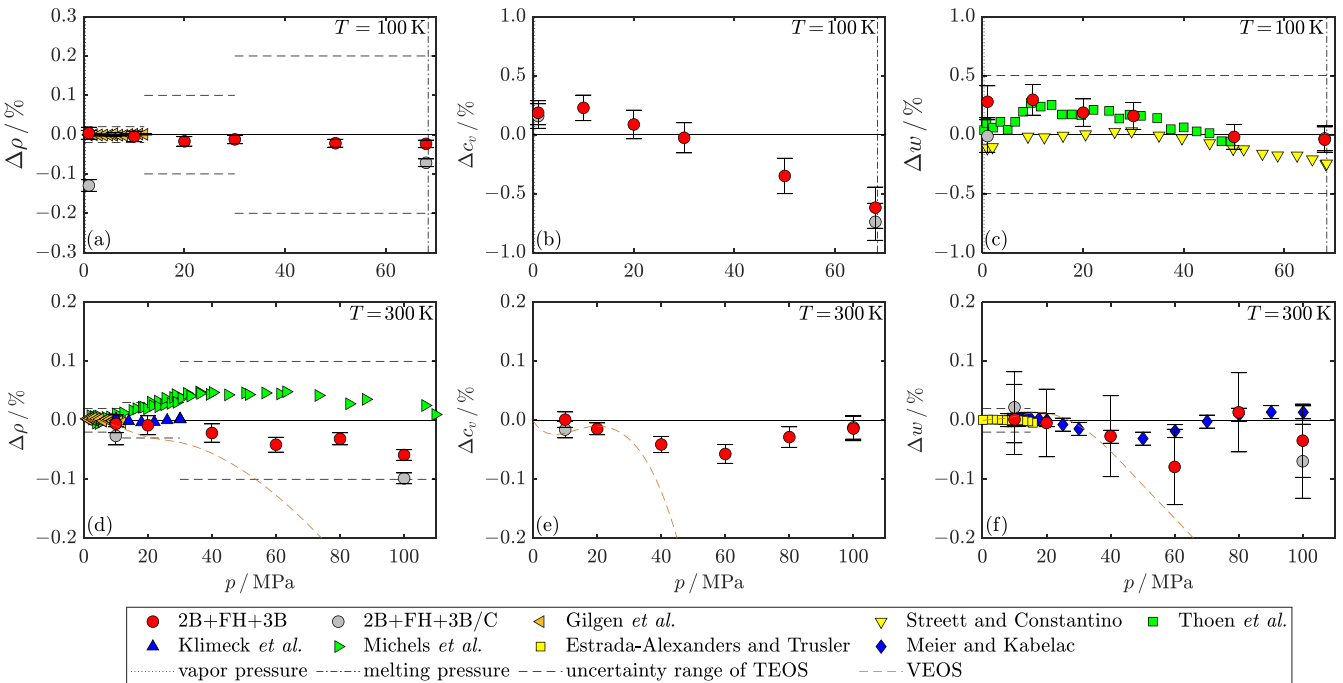


FIG. 3. Relative deviations of our results for model 2B+FH+3B and experimental data from the literature for the density, isochoric heat capacity, and speed of sound at 100 and 300 K from the TEOS as a function of pressure  $p$  (a)–(f).

ensemble derived using the Lustig methodology should be applied. When computationally expensive *ab initio* two-body and nonadditive three-body potentials are employed to model the interactions between the particles, the isothermal-isobaric ensemble is particularly advantageous because the expressions for the properties contain no volume derivatives of the enthalpy.

Second, if *ab initio* two-body and nonadditive three-body potentials describe the second and third virial coefficients of a noble gas accurately, they are also capable of predicting very accurate values of all thermodynamic properties in a large part of the fluid region. Nonadditive three-body interactions and quantum effects yield significant contributions to thermodynamic properties in the liquid and supercritical regions. Nonadditive three-body interactions contribute the most near the vapor-liquid phase boundary, while quantum effects must especially be accounted for at low temperatures.

Third, to obtain properties of macroscopic systems, a series of simulations with several particle numbers must be carried out at each state point. The results of the simulations must be extrapolated into the thermodynamic limit.

Fourth, the uncertainty of the potentials must in principle also be taken into account in the uncertainty estimate for a property. Because it was the aim of this work to demonstrate the capability of the Lustig methodology in combination with *ab initio* potentials and not yet to generate reference data with well-defined uncertainties for argon, this contribution to the uncertainty was outside the scope of this work.

Finally, it is straightforward to extend the procedure developed here to fluids consisting of rigid linear and nonlinear molecules using *ab initio* potentials. Nonrigid molecules would usually require a full quantum formulation of statistical mechanics instead of a classical or semiclassical formulation as applied in this work.

### ACKNOWLEDGMENT

We thank our former colleague Johann-Philipp Crusius for preliminary work within his dissertation [48] on the feasibility of obtaining accurate values of thermodynamic properties from Monte Carlo simulations with *ab initio* potentials.

- 
- [1] E. Ermakova, J. Solca, H. Huber, and M. Welker, *J. Chem. Phys.* **102**, 4942 (1995).
- [2] J. Solca, A. J. Dyson, G. Steinebrunner, B. Kirchner, and H. Huber, *Chem. Phys.* **224**, 253 (1997).
- [3] T. Pfeleiderer, I. Waldner, H. Bertagnolli, K. Tödheide, B. Kirchner, H. Huber, and H. E. Fischer, *J. Chem. Phys.* **111**, 2641 (1999).
- [4] J. A. Anta, E. Lomba, and M. Lombardero, *Phys. Rev. E* **55**, 2707 (1997).
- [5] K. Leonhard and U. K. Deiters, *Mol. Phys.* **98**, 1603 (2000).
- [6] A. E. Nasrabad, R. Laghaei, and U. K. Deiters, *J. Chem. Phys.* **121**, 6423 (2004).
- [7] A. E. Nasrabad and R. Laghaei, *J. Chem. Phys.* **125**, 084510 (2006).
- [8] R. Bukowski and K. Szalewicz, *J. Chem. Phys.* **114**, 9518 (2001).
- [9] G. Marcelli and R. J. Sadus, *J. Chem. Phys.* **111**, 1533 (1999).
- [10] G. Marcelli and R. J. Sadus, *J. Chem. Phys.* **112**, 6382 (2000).
- [11] L. Wang and R. J. Sadus, *Phys. Rev. E* **74**, 031203 (2006).
- [12] L. Wang and R. J. Sadus, *J. Chem. Phys.* **125**, 144509 (2006).
- [13] M. Vlasiuk and R. J. Sadus, *J. Chem. Phys.* **146**, 244504 (2017).
- [14] M. Vlasiuk and R. J. Sadus, *J. Chem. Phys.* **147**, 024505 (2017).
- [15] A. Malijevský and A. Malijevský, *Mol. Phys.* **101**, 3335 (2003).
- [16] E. Pahl, F. Calvo, L. Koči, and P. Schwerdtfeger, *Angew. Chem. Int. Ed.* **47**, 8207 (2008).
- [17] U. K. Deiters and R. J. Sadus, *J. Chem. Phys.* **150**, 134504 (2019).
- [18] U. K. Deiters and R. J. Sadus, *J. Phys. Chem. B* **125**, 8522 (2021).
- [19] B. M. Axilrod and E. Teller, *J. Chem. Phys.* **11**, 299 (1943).
- [20] Y. Muto, *Nippon Sugaku-Buturigakukai-si* **17**, 629 (1943).
- [21] R. Lustig, Habilitationsschrift, RWTH Aachen, Aachen, Germany, 1994.
- [22] R. Lustig, *J. Chem. Phys.* **100**, 3048 (1994).
- [23] R. Lustig, *J. Chem. Phys.* **100**, 3060 (1994).
- [24] R. Lustig, *J. Chem. Phys.* **100**, 3068 (1994).
- [25] R. Lustig, *J. Chem. Phys.* **109**, 8816 (1998).
- [26] R. Lustig, *Mol. Simul.* **37**, 457 (2011).
- [27] R. Lustig, *Mol. Phys.* **110**, 3041 (2012).
- [28] P. Ströker, R. Hellmann, and K. Meier, *Phys. Rev. E* **103**, 023305 (2021).
- [29] B. Jäger, R. Hellmann, E. Bich, and E. Vogel, *Mol. Phys.* **107**, 2181 (2009); **108**, 105 (2010).
- [30] R. P. Feynman and A. R. Hibbs, *Quantum Mechanics and Path Integrals* (McGraw-Hill, New York, 1965).
- [31] E. Vogel, B. Jäger, R. Hellmann, and E. Bich, *Mol. Phys.* **108**, 3335 (2010).
- [32] B. Jäger, R. Hellmann, E. Bich, and E. Vogel, *J. Chem. Phys.* **135**, 084308 (2011).
- [33] K. T. Tang and J. P. Toennies, *J. Chem. Phys.* **80**, 3726 (1984).
- [34] B. Jäger, *Z. Phys. Chem.* **227**, 303 (2013).
- [35] W. Cencek, G. Garberoglio, A. H. Harvey, M. O. McLinden, and K. Szalewicz, *J. Phys. Chem. A* **117**, 7542 (2013).
- [36] N. Metropolis, A. W. Rosenbluth, M. N. Rosenbluth, A. H. Teller, and E. Teller, *J. Chem. Phys.* **21**, 1087 (1953).
- [37] M. P. Allen and D. J. Tildesley, *Computer Simulation of Liquids* (Clarendon, Oxford, UK, 1987).
- [38] Joint Committee for Guides in Metrology, JCGM 101:2008, *Evaluation of measurement data—Supplement 1 to the “Guide to the expression of uncertainty in measurement”—Propagation of distributions using a Monte Carlo method* (Bur. Intl. Poids et Mesures, Sèvres, France, 2008).
- [39] See Supplemental Material at <http://link.aps.org/supplemental/10.1103/PhysRevE.105.064129> for tabulated simulation results for all models and figures showing the extrapolation of simulation results into the thermodynamic limit and deviations of further thermodynamic properties from the TEOS.
- [40] C. Tegeler, R. Span, and W. Wagner, *J. Phys. Chem. Ref. Data* **28**, 779 (1999).

- [41] R. Gilgen, R. Kleinrahm, and W. Wagner, *J. Chem. Thermodyn.* **26**, 383 (1994).
- [42] J. Klimeck, R. Kleinrahm, and W. Wagner, *J. Chem. Thermodyn.* **30**, 1571 (1998).
- [43] A. Michels, H. Wijker, and H. K. Wijker, *Physica* **15**, 627 (1949).
- [44] A. F. Estrada-Alexanders and J. P. M. Trusler, *J. Chem. Thermodyn.* **27**, 1075 (1995).
- [45] W. B. Streett and M. S. Constantino, *Physica* **75**, 283 (1974).
- [46] J. Thoen, E. Vangeel, and W. Van Dael, *Physica* **45**, 339 (1969).
- [47] K. Meier and S. Kabelac, *Rev. Sci. Instrum.* **77**, 123903 (2006).
- [48] J.-P. Crusius, Dissertationsschrift, Universität Rostock, Rostock, Germany, 2016.